Magnetotransport in nanostructures: The role of inhomogeneous currents

Tiago S. Machado,[1] M. Argollo de Menezes,[2] Tatiana G. Rappoport,[3] and Luiz C. Sampaio[1,a)]
[1]*Centro Brasileiro de Pesquisas Físicas, Xavier Sigaud, 150, Rio de Janeiro, RJ, 22.290-180, Brazil*
[2]*Instituto de Física, Universidade Federal Fluminense, Rio de Janeiro, RJ, 24.210-346, Brazil*
[3]*Instituto de Física, Universidade Federal do Rio de Janeiro, Rio de Janeiro, RJ, 68.528-970, Brazil*

(Received 4 January 2011; accepted 27 March 2011; published online 3 May 2011)

In the study of electronic transport in nanostructures, electric current is commonly considered homogeneous along the sample. We use a method to calculate the magnetoresistance of magnetic nanostructures where the current density may vary in space. The current distribution is numerically calculated by combining micromagnetic simulations with an associated resistor network and by solving the latter with a relaxation method. As an example, we consider a Permalloy disk exhibiting a vortex-like magnetization profile. We find that the current density is inhomogeneous along the disk, and that during the core magnetization reversal it is concentrated toward the center of the vortex and is repelled by the antivortex. We then consider the effects of the inhomogeneous current density on spin-torque transfer. The numerical value of the critical current density necessary to produce a vortex core reversal is smaller than the one that does not take the inhomogeneity into account. © *2011 American Institute of Physics*. [doi:10.1063/1.3582149]

I. INTRODUCTION

Electric transport in magnetic nanostructures is a useful tool both for probing and for manipulating the magnetization. In the low current density regime, magnetoresistance curves are useful for probing the sample's magnetization state while, in the high current density regime, magnetization patterns can be modified by a spin-transfer torque.[1–3] Magnetoresistance measurements have the advantage of being relatively simple and fast, serving as an efficient magnetic reading mechanism.[4,5]

Depending upon their thickness and diameter, small ferromagnetic disks exhibit stable topological defects known as magnetic vortices.[6,7] These vortices can be manipulated by picosecond pulses of a few (tens of) oersted in-plane magnetic fields that switch their polarity,[8–13] making them good candidates for elementary data storage units.[9]

For their use as storage units, the most viable form of manipulation of the magnetization is through spin-torque transfer, with the injection of high density electrical currents.[1] The effect of these currents in the magnetization dynamics is described theoretically by the incorporation of adiabatic and nonadiabatic spin-torque terms in the Landau-Lifshitz-Gilbert (LLG) equation.[14,15] These two terms are proportional to the injected current density and it is normally considered an homogeneous current distribution inside the disk. Although theoretical predictions using this approach qualitatively agree with experimental results, there is a lack of quantitative agreement between theoretical and experimental results regarding the current densities necessary to modify the magnetic structures.[17–19]

In this paper we investigate the effect of nonuniform current distributions on electronic transport and spin-torque transfer in ferromagnetic systems exhibiting vortices. We numerically calculate the magnetoresistance (MR) and local current distribution of a ferromagnetic disk by separating the time scales for magnetic ordering and electronic transport. We consider an effective anisotropic magnetoresistance (AMR) that depends on the local magnetization. We discretize the disk in cells and solve the Landau-Lifshitz-Gilbert (LLG) equation[20] numerically with the fourth-order Runge-Kutta,[21] thereby obtaining the magnetization profile of the disk. This pattern is used to calculate the magnetoresistance of each cell as a fixed current, I, is applied at two symmetrically distributed electrical contacts, resulting in a voltage drop and an inhomogeneous current distribution along the disk.

This method couples the electric and magnetic properties of the metallic nanomagnets and can be used to analyze the effect of inhomogeneous current distributions in different contexts. First, we discuss the limit of low current density where transport measurements can be used to probe the magnetic structure. We compare the magnetic structure with the magnetoresistance curves and show how the magnetoresistance measurements could be interpreted to obtain information on the magnetization profile and its dynamics during the vortex core magnetization reversal. Moreover, we discuss the consequences of a nonhomogeneous current distribution on the spin-torque transfer and find that the critical current density that produces the vortex core reversal is reduced by one order of magnitude whenever such noninhomogeneity is taken into account. This result can be seen as a new route to understanding why the experimental values of the critical current densities are usually lower than the ones obtained in the LLG calculations.[17–19]

This article is organized as follows: In Sec. II we discuss the model and method for the calculation of the magnetoresistance and current distribution. In Sec. III, we exemplify the calculations by considering the magnetoresistance and current distributions of a Permalloy disk exhibiting a

a)Author to whom correspondence should be addressed. Electronic mail: sampaio@cbpf.br.

magnetic vortex. In Sec. IV, we study the consequences of a nonhomogeneous current distribution on the spin-torque transfer. In Sec. V we summarize the main results.

II. MAGNETORESISTANCE AND CURRENT DISTRIBUTION CALCULATIONS

Let us consider a 36 nm-thick Permalloy disk with a diameter of 300 nm discretized into a grid of $4 \times 4 \times 4$ nm^3 cells. The dynamics of the magnetization vector associated with each cell is given by the Landau-Lifshitz-Gilbert equation, which we numerically integrate with the fourth-order Runge-Kutta and discretization step, $h = 10^{-4}$.[21] The parameters associated with the LLG equation are the saturation magnetization $M_s = 8.6 \times 10^5$ A/m, the exchange coupling, $A = 1.3 \times 10^{-11}$ J/m, and the Gilbert damping constant $\alpha = 0.05$.[13]

By varying the external in-plane magnetic field, H, from negative to positive saturation we obtain a hysteresis curve, as depicted in Fig. 1, which is consistent with experimental observations.[7] As shown in Fig. 1(a), in static equilibrium and in the absence of magnetic fields, a vortex structure with a core magnetized perpendicular to the disk plane is formed in the center of the disk. If a small in-plane magnetic field, H, is applied, the core is displaced from the center [Fig. 1(b)]. At a critical field, H_{c1}, the vortex is expelled from the disk, resulting in a discontinuity in the hysteresis loop. As the external field, H, is lowered back, the vortex structure reappears, but at a lower field, $H_{c2} < H_{c1}$.

In order to investigate the electronic transport on the nanomagnetic disk we consider the magnetization profile, $\{\vec{M}_i\}$, obtained as the stationary solution of the LLG equation, as a starting point to calculate the magnetoresistance, R_i, in each cell, i, of the disk. It is well established that in relatively clean magnetic metals the main source of magnetoresistance is the anisotropic magnetoresistance (AMR),[22] which can be expressed as $\rho = \rho^{\perp} + (\rho^{\parallel} - \rho^{\perp})\cos^2\varphi$, where φ is the angle between the local magnetization and the electric current and $\rho^{\perp}$ and $\rho^{\parallel}$ are the resistivities when the magnetization is perpendicular and parallel to the current, respectively. We decompose the current into orthogonal components, x and y, such that if the normalized projection of the magnetization, $\vec{M}_i$, on the current direction $\hat{u}$ ($u = x, y$) is $m_i^u = \cos\varphi$, and the cell geometrical factor is taken into account, the magnetoresistance, R_i, is split into orthogonal components as $R_i^u = R_i^{\perp} + (R_i^{\parallel} - R_i^{\perp})(m_i^u)^2$ in every cell, i, of the disk (Fig. 2). Thus, we obtain a resistor network where the resistances depend on the local magnetization and are assumed to be approximately constant at the time scale of electronic scattering processes.

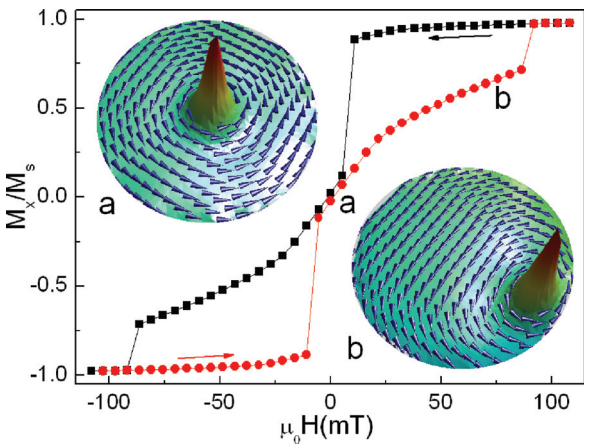

FIG. 1. (Color online) Magnetic hysteresis obtained with a micromagnetic simulation of a Permalloy disk with a diameter of 300 nm and a thickness of 36 nm, subject to a static in-plane magnetic field, H. Two configurations for the vortex core, corresponding to different external fields (0 and 75 mT), are also depicted.

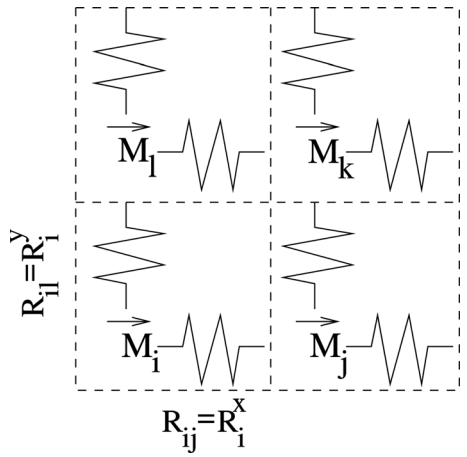

FIG. 2. Original cells used in the LLG simulation with the associated resistance network.

Guided by recent experiments[23] we allow a constant current, I, to flow along the disk by attaching symmetrically

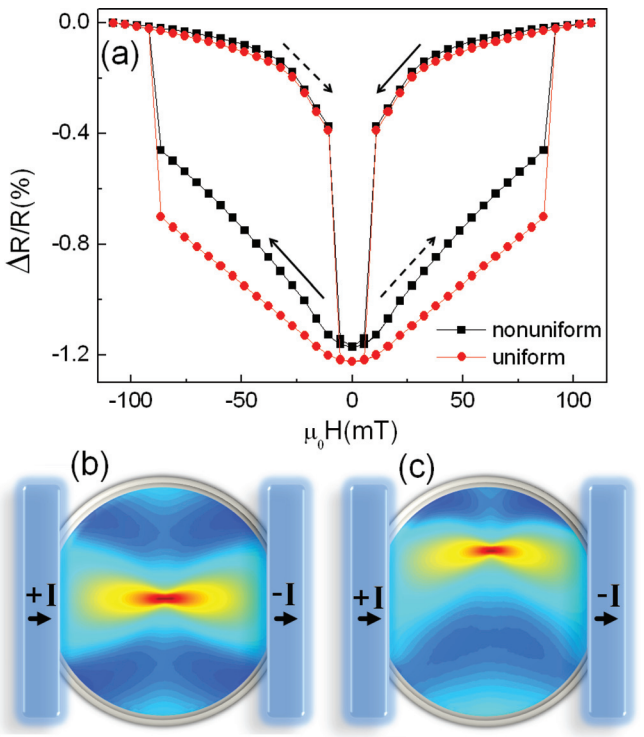

FIG. 3. (Color online) (a) Magnetoresistance for the magnetic configurations obtained in Fig. 1 for uniform (circle) and nonuniform (square) current distribution. Bottom: electric current map for (b) zero field and (c) $H = 75$ mT. The red (blue) color corresponds a current density which is about $1 - 2\%$ larger (smaller) than the uniform current at the saturation field. The red color is in the center of the vortex.

placed electrodes on it (see Fig. 3). The voltage drop along the resistors and the associated current map of the disk are obtained by solving Kirchhoff's equation iteratively at each node of the grid with a relaxation method[24,25]

$$V_i^{(n+1)} = \left(\sum_{(j)} 1/R_{ij}\right)^{-1} \left(\sum_{(j)} \frac{V_j^{(n)}}{R_{ij}} + b_i\right), \qquad (1)$$

where R_{ij} is $R_i^x(R_i^y)$ if i and j are horizontal (vertical) neighbors and b_i is the boundary current, assumed to be $I(-I)$ at the leftmost (rightmost) cells, and zero otherwise (see Fig. 2). Here, V_i^n is the voltage at site i after n iterations and the sums run over the nearest-neighbors (j) of node i. Starting with a random initial condition, $\{V_i^{(0)}\}$, at each site we iterate Eq. (1) until each $V_i^{(n)}$ becomes stationary (within 9 decimal digits precision). After convergence, we calculate the equivalent resistance, the ratio, $R_{\mathrm{eq}} = \Delta V/I$, between the voltage drop, ΔV, between the electrodes, given by

$$\Delta V = \sum_{i\|b_i=I} V_i - \sum_{j\|b_j=-I} V_j, \qquad (2)$$

and the current, I, entering the disk.

III. MAGNETO-STRUCTURE AND MAGNETORESISTANCE

A. Hysteresis and magnetoresistance

In order to obtain the magnetoresistance curves, the calculation discussed in the previous section is performed at different fields. The magnetoresistance and current distribution for the same points of the hysteresis loop in Fig. 1 are depicted in Fig. 3. Figure 3(a) displays the magnetoresistance curves for both homogeneous (without using the resistance network[26]) and nonhomogeneous current distributions. The vortex expulsion and its formation at a different critical field are clearly identified and, with $\rho^{\|} = 155\ \Omega\,\mathrm{nm}$ and $\rho^{\perp} = 150\ \Omega\,\mathrm{nm}$, we obtain a MR of 1.2% for the nonhomogeneous distribution, which is a typical value found in previous experiments.[23,27]

One also observes that the magnetoresistance curves for uniform and nonuniform current distributions differ significantly, the latter being more comparable to experimental results with the same contact geometry.[23] As expected, a homogeneous current overestimates the magnetoresistance, since the current will flow through regions of high resistance, whereas with the current found by solving Laplace's equation on the associated resistor network, one finds a preferential path (higher current density) on regions of low resistance. This difference is more pronounced in the presence of a vortex, since the magnetization of the disk is highly nonhomogeneous on such configurations.

In light of the discussion above, one sees in Figs. 3(b) and 3(c) that the current is not homogeneously distributed inside the disk, being stronger toward the center of the vortex core. In the center of the disk the magnetization either points in the $\hat{z}$ direction, perpendicular to the direction of current flow, or loops about the vortex core. In both cases, the current has a path where its direction is always perpendicular to the magnetization, reducing the local magnetoresistance. Above the saturation field, the magnetization is uniform and at the disk center the same applies to the current. The red (blue) region has a current density $1-2\%$ larger (smaller) than the current, I, at saturation. The red region is in the center of the vortex. This effect might be enhanced if other sources of magnetoresistance are considered, such as giant magnetoresistance, for example. Similar approaches using different sources of magnetoresistance and geometries have been used to calculate the magnetoresistance in nanomagnets.[27–32]

B. Dynamics

Next, we study the dynamics of the vortex core magnetization reversal by the application of short in-plane magnetic fields. Under a pulsed in-plane magnetic field or spin polarized current excitation, the vortex with a given polarity (V^+) dislocates from the center of the disk with the nucleation of a vortex (V^-)-antivortex (AV^-) pair with opposite polarity after the vortex attains a critical velocity of rotation about the disk center.[3,33] The original V^+ then annihilates with the AV^-, and a vortex with reversed core magnetization (V^-) (Ref. 9) remains. If a low-density electronic current is made to flow through the sample (without disturbing the magnetization dynamics), we observe changes in the magnetoresistance, as the vortices nucleate and annihilate. In Fig. 4(a) we depict the dynamics of the magnetoresistance as a pulsed in-plane magnetic field is applied in the $\hat{x}$ direction at $t = 20$ ps for different pulse intensities. The pulses have their shape sketched in gray in Fig. 4(a) with a full width at half maximum of $t = 250$ ps. Depending on the pulse intensity, the vortex core magnetization does not reverse at all ($\mu_0 H < 43$ mT), reverses once ($54\ \mathrm{mT} < \mu_0 H < 64$ mT), or multiple times ($\mu_0 H > 64$ mT).[12,13]

During the application of a field pulse in the $\hat{x}$ direction, i.e., parallel to the current flow, the vortex core is pushed to the $\hat{y}$ direction, breaking the rotation symmetry of the disk's magnetization, increasing both the total m_x component and the disk's equivalent resistance [see Fig. 4(a)]. At $t = 340$ ps, the field is practically zero and, from the decay of the magnetoresistance to its equilibrium (initial) value, one can infer whether there was reversal of the vortex core polarization or not: for pulses that induce reversal, the value of the magnetoresistance just after the pulse is always larger than its initial value. If there is no reversal the magnetoresistance attains a minimum value that is lower than its initial value, i.e., before the application of the pulse, and oscillates about it.

In Figs. 4(b)–4(e) we depict snapshots of current (color map) and magnetization (arrows) distributions at time steps marked with black dots in Fig. 4(a), in situations with or without vortex core magnetization reversal. Whenever the pulse decreases its intensity, the total m_x component and the equivalent resistance of the disk follow the same pattern (although with some time delay), because the vortex core tends to return to the disk center, where $m_x = 0$. Figure 4(b) shows the current distribution and magnetization at a moment corresponding to the minimum of the resistance curve, for a field intensity, $\mu_0 H = 27$ mT, for which there is

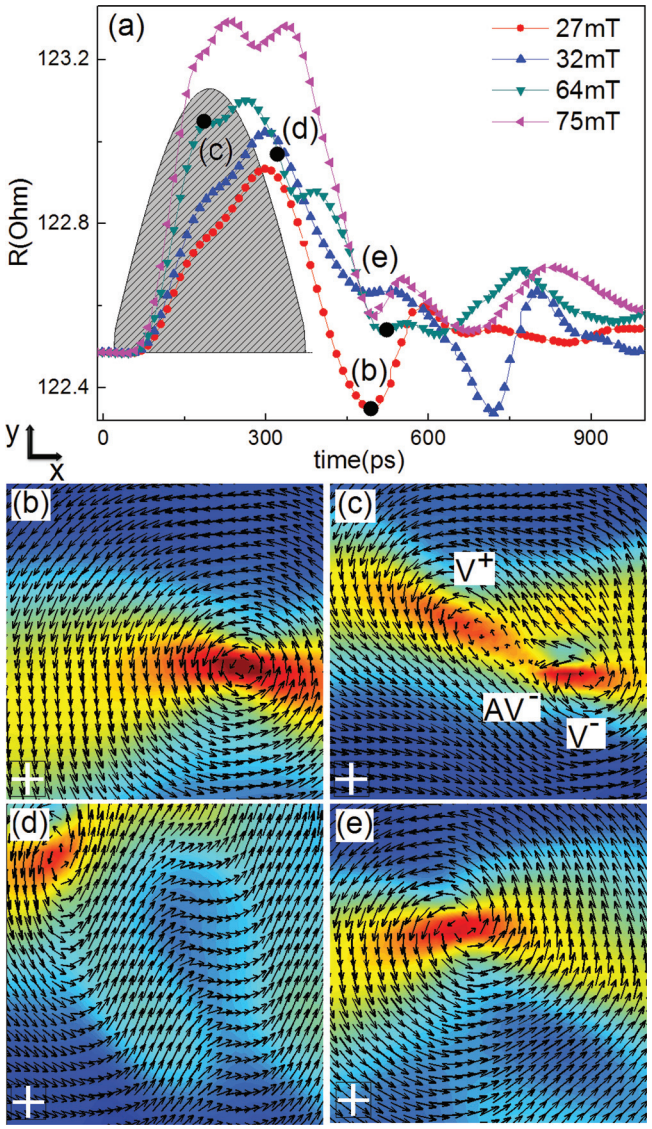

FIG. 4. (Color online) (a) Evolution of magnetoresistance after the application of pulsed in-plane magnetic fields (the shape is shown in gray) with different intensities. Snapshots of magnetization (arrows) and current distribution (color map) for pulse fields (b) without and (c)–(e) with (a vortex core magnetization reversal. The white cross shows the position of the disk center. Both the current and the magnetic field are applied in the $\hat{x}$ direction.

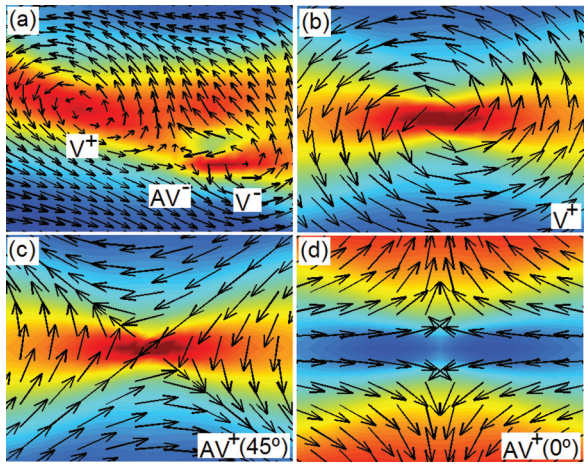

FIG. 5. (Color online) (a)–(d) Snapshots of magnetization (arrows) and current distribution (color map) of (a) the vortex core magnetization reversal process at $t = 214$ ps, (b) a vortex and its associated current distribution, and (c) and (d) antivortices rotated by 45° with respect to each other and their associated current distribution. Depending on the relative orientation of the antivortex it can either focus (c) or repel (d) currents away from the center of the core.

no vortex core reversal. There is a large region with m_y magnetization (and small m_x) in the center of the disk. This region, together with the vortex core, creates a low resistance path for the electronic current, decreasing the equivalent resistance toward a value below the equilibrium resistance. Figures 4(c)–4(e) show the magnetization and current distributions at different moments of the vortex core magnetization reversal for a situation where there is a single reversal ($\mu_0 H = 64$ mT). In Fig. 4(c) we depict the current distribution at the exact moment of nucleation of the V^- -AV^- pair, the initial stage of vortex core magnetization reversal. Figure 4(d) shows the spin waves emitted just after the V^+ -AV^- annihilation, which is a process that occurs with energy dissipation. Such energy loss drives the vortex core to the disk center along with some small oscillations, mainly due to the reflections of spin waves at the edges of the disk. It turns out that the resistance follows an equivalent behavior: it decreases toward the initial resistance value and remains always above it. Figure 4(e) shows the current distribution after the field pulse has vanished. As can be seen, the time dependent resistance curves can give us an indication of the vortex reversal process.

Let us discuss in further detail the interplay between the magnetization pattern and the current distribution. In Fig. 5 (a) we show a snapshot of the current distribution during the vortex core magnetization reversal process, with the V^+ and the V^--AV^- pair with negative polarity. As shown in Figs. 3, 4, and 5(b) the current is pushed to the vortex core, where $m_x = 0$ and, consequently, the local resistance is minimum. With the nucleation of the AV^- vortex [Fig. 5(a)], m_x becomes larger than zero around it, with $m_y \to 0$. As the current flows in the $\hat{x}$ direction, it is repelled from the antivortex core.

In the latter analysis we considered a particular orientation of the AV. However, as can be seen in Figs. 5(c) and 5(d), depending on their orientation, antivortices can either attract (in the first case) or repel currents (in the latter case). Vortices are rotation invariant, and always attract current toward their cores. It is important to point out that this difference in current distributions might have important consequences in the high-density current spin-torque transfer acting on either a vortex or an antivortex. For instance, although the inversion process through spin-torque for an AV is equivalent to the one for a V, we should expect different current densities in each one, since currents can only penetrate the AV core at a particular orientation.

IV. SPIN-TORQUE TRANSFER

In this section, we discuss the consequences of inhomogeneous currents in the spin-torque transfer. In order to determine how the current distribution is incorporated in the spin-torque terms of the modified LLG equation, we need to review a few steps of their derivations. It is important to note that in our approach, the only source of nonhomogeneous

current distribution is the anisotropic magnetoresistance, as discussed in Sec. II. All other effects are neglected.

The itinerant electron spin operator satisfies the continuity equation

$$\frac{d}{dt}\langle \boldsymbol{s}\rangle + \nabla \cdot \langle \hat{\boldsymbol{J}}\rangle = -\frac{\boldsymbol{i}}{\hbar}(\langle [\boldsymbol{s}, \boldsymbol{H}]\rangle) \tag{3}$$

where $\boldsymbol{J}$ is the spin current operator. The Hamiltonian, H, is the s-d Hamiltonian ($H_{sd} = -J_{ex}\boldsymbol{s}\cdot\boldsymbol{S}$), where s and $S/S = -\boldsymbol{M}/M_s$ are the spins of itinerant and localized electrons, and J_{ex} is the exchange coupling strength between them. We define the spin current density, $\boldsymbol{J} = \langle \hat{\boldsymbol{J}}\rangle = -(g\mu_B P/eM_s)\boldsymbol{j}_e(\boldsymbol{r}) \otimes \boldsymbol{M}$, where $\boldsymbol{j}_e(\boldsymbol{r})$ is the current density, and the electron spin density is given by $\boldsymbol{m} = \langle \boldsymbol{s}\rangle$.[14] We use the same approximations previously used to calculate the spin-torque,[14,15] with the new ingredient of nonhomogeneous current density. We obtain

$$\frac{d}{dt}\boldsymbol{m} = \frac{\mu_b P}{eM_s}\{\boldsymbol{M}[\nabla \cdot \boldsymbol{j}_e(\boldsymbol{r})] + [\boldsymbol{j}_e(\boldsymbol{r})\cdot\nabla]\} - \frac{J_{ex}S}{M_s}\boldsymbol{m}\times\boldsymbol{M}, \tag{4}$$

where $\boldsymbol{M}$ is the matrix magnetization, g is the Landé factor splitting, μ_B is the Bohr magneton, P is the spin current polarization of the ferromagnet, and e is the electron charge. From the continuity equation for charges, the term containing $\nabla\cdot\boldsymbol{j}_e(\boldsymbol{r})$ is always zero, even if the current density is not constant. As we discussed previously, the same divergent is used to determine the current distribution in Sec. II. This expression is exactly the same expression obtained previously, but with $\boldsymbol{j}_e(\boldsymbol{r})$ in the second term of the right hand side of the equation varying with $\boldsymbol{r}$. This current distribution is introduced at the modified LLG that considers spin-torque transfer. Therefore, we obtain a spin-torque transfer where the current distribution is not uniform.

To consider the spin-torque transfer effects we include adiabatic and nonadiabatic spin torque terms in the LLG equation,

$$\frac{d}{dt}\boldsymbol{m} = -\gamma_0\boldsymbol{m}\times\boldsymbol{H}_{\text{eff}} + \alpha\boldsymbol{m}\times\frac{d}{dt}\boldsymbol{m} - (\boldsymbol{u}\cdot\nabla)\boldsymbol{m} + \beta\boldsymbol{m}\times[(\boldsymbol{u}\cdot\nabla)\boldsymbol{m}], \tag{5}$$

where, $\mathbf{m} = \mathbf{M}/M_s$ is the normalized local magnetization, α is a phenomenological damping constant, γ_0 is the gyroscopic ratio, and $\mathbf{H}_{\text{eff}}$ is the effective field, which is composed of the applied external field, the demagnetization field, the anisotropy field, and the exchange field. The first term describes the precession of the normalized local magnetization about the effective field. The second term describes the relaxation of the normalized local magnetization and β is a dimensionless parameter that describes the strength of the nonadiabatic term, which we consider to be 0.5.[15,16] The velocity $\mathbf{u}(\mathbf{r}) = (gP\mu_B/2eM_s)\,\mathbf{j}_e(\mathbf{r})$ is a vector pointing parallel to the direction of the electron flow and $\mathbf{j}_e(\mathbf{r})$ is calculated using the procedure discussed in Sec. II.

To explain the importance of our assumption about the current distribution let us analyze the critical current density, $\boldsymbol{j}_e^c$, which is the minimal current density needed to produce a vortex core reversal. For this purpose, we simulated the magnetization dynamics of a system subjected to a DC current with the modified LLG equation [Eq. (5)]. In Fig. 6(a) one sees the vortex core polarity as a function of current density, $\boldsymbol{j}_e$. The different curves represent situations of homogeneous current (squares) and three different values of AMR where the magnetoresistance ranges from 2 to 10%. Such AMR, as discussed in the previous sections, determines the degree of current inhomogeneity throughout the disk. One can see that the critical current density, $\boldsymbol{j}_e^c$ in our model is $3-10\%$ smaller than the one obtained for uniform currents. These results suggest a new route, together with the nonadiabatic term, to explain the discrepancy between the experimental results and theoretical calculations of the critical current density, $\boldsymbol{j}_e^c$.

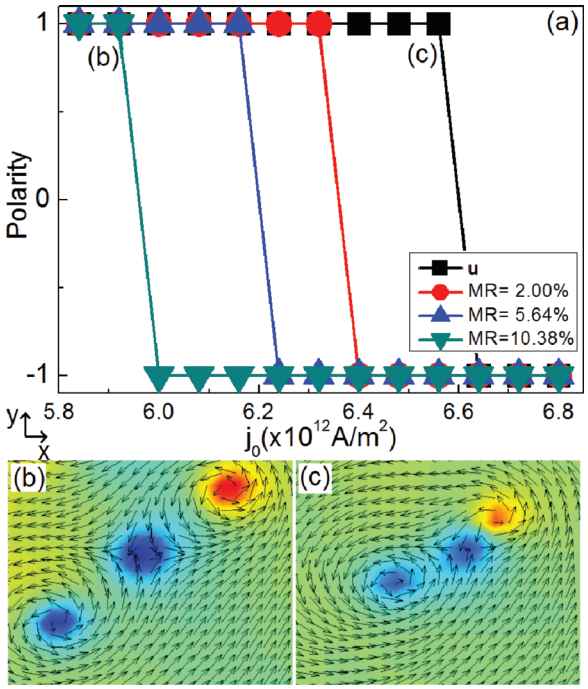

FIG. 6. (Color online) (a): Core polarity as a function of current density for homogeneous (squares) and nonhomogeneous current distributions (with different MR). (b) and (c): Magnetization profiles during the inversion process at the critical current for both (b) nonhomogeneous and (c) homogeneous (c) current distributions. The color map represent the out-of-plane magnetization, m_z, and the arrows represent the in-plane component.

Even though the value of $\boldsymbol{j}_e^c$ is reduced, the vortex-core reversal process for nonhomogenous current distributions is similar to the homogenous case. Figures 6(b) and 6(c) show the magnetic configurations for the moment just before the V^+-AV^- annihilation, at the critical current density, for the model with nonhomogeneous and homogeneous current distributions, respectively. In the case of inhomegeneous currents, the fact that a V(AV) attracts (repels) the current affects the velocity and separation distance of the V-AV pair during the vortex core reversal. As the vortices attract current, the current densities at their core are higher than the average and can reach values higher than $\boldsymbol{j}_e^c$ of the homogenous case. As a result, the vortex gains the necessary velocity to produce the vortex core switching for a lower $\boldsymbol{j}_e^c$.

Alternatively, as the antivortices repel currents, the current density at their core is smaller, making them slower thanthe vortices. As a result, after the nucleation of the V^{-}-AV^{-} pair, their separation occurs faster than in the case where the current density in the center of a V or an AV is the same, as is usually considered in micromagnetic simulations. Consequently, not only is j_e^c reduced, but the inversion time is also reduced.

Our analysis might also have important technological implications, since we observe a (almost linear) correlation between the current density necessary to produce a core inversion and the anisotropic magnetoresistance of the material. Thus, by increasing the AMR of the sample, one can decrease the critical current, j_e^c, which is strongly desirable in memory devices for the sake of low energy comsumption and minimal heat waste.

V. CONCLUSIONS

We performed a realistic calculation of the magnetoresistance effects in magnetic nanostructures that takes into account inhomogeneous current densities. For that purpose, we adapted a numerical relaxation scheme for the Laplace equation to the solution of the LLG equation for the magnetization profile along a Permalloy disk. Our results suggest that resistance measurements might be useful to probe the dynamics of the vortex core magnetization reversal, induced by short in-plane magnetic pulses. Moreover, we note that the difference between current distributions close to the vortices and anti-vortices have significant consequences for the spin-torque transfer effect. The inhomogeneous current distribution inside the magnet substantially reduces the critical current density necessary to produce a vortex core reversal. We conclude that materials with large anisotropic magnetoresistance need lower current densities to modify their magnetic structure, a much desired feature for most modern memory devices.

ACKNOWLEDGMENTS

This work was supported by CNPq and FAPERJ. L.C.S. and T.G.R. acknowledge the ''INCT de Fotônica'' and ''INCT de Informacão Quântica'', respectively, for financial support.

[1]J. C. Slonczewski, J. Magn. Magn. Mater. **159**, L1 (1996); L. Berger, Phys. Rev. B **54**, 9353 (1996).
[2]D. C. Ralph and M. D. Stiles, J. Magn. Magn. Mater **320**(7), 1190 (2008).
[3]K. Yamada, S. Kasai, Y. Nakatani, K. Kobayashi, H. Kohno, A. Thiaville, T. Ono, and O. Teruo, Nature Mater. **6**, 269 (2007).
[4]I. N. Krivorotov, N. C. Emley, J. C. Sankey, S. I. Kiselev, D. C. Ralph, and R. A. Buhrman, Science **307**, 215 (2005).
[5]S. Choi, K.-S. Lee, and S.-K. Kim, Appl. Phys. Lett. **89**, 062501 (2006).
[6]T. Shinjo, T. Okuno, R. Hassdorf, K. Shigeto, and T. Ono, Science **289**, 930 (2000).
[7]R. P. Cowburn, D. K. Koltsov, A. O. Adeyeye, M. E. Welland, and D. M. Tricker, Phys. Rev. Lett. **83**, 1042 (1999).
[8]M. Weigand, B. Van Waeyenberge, A. Vansteenkiste, M. Curcic, V. Sackmann, H. Stoll, T. Tyliszczak, K. Kaznatcheev, D. Bertwistle, G. Woltersdorf, C. H. Back, and G. Schutz, Phys. Rev. Lett. **102**, 077201 (2009).
[9]A. Vansteenkiste, K. W. Chou, M. Weigand, M. Curcic, V. Sackmann, H. Stoll, T. Tyliszczak, G. Woltersdorf, C. H. Back, G. Schütz, and B. Van Waeyenberge, Nature (London) **5**, 332 (2009).
[10]B. Van Waeyenberger, A. Puzic, H. Stoll, K. W. Chou, T. Tyliszczak, R. Hertel, M. Fahnle, H. Bruckl, K. Rott, G. Reiss, I. Neudecker, D. Weiss, C. H. Back, and G. Schutz, Nature (London) **444**, 461 (2006).
[11]R. Hertel, S. Gliga, M. Fähnle, and C. M. Schneider, Phys. Rev. Lett. **98**, 117201 (2007).
[12]S. K. Kim, K. S. Lee, Y. S. Yu, and Y. S. Choi, Appl. Phys. Lett. **92**, 022509 (2008); K. S. Lee, K. Y. Guslienko, J. Y. Lee, and S. K. Kim, Phys. Rev. B **76**, 174410 (2007).
[13]T. S. Machado, T. G. Rappoport, and L. C. Sampaio, Appl. Phys. Lett. **93**, 112507 (2008).
[14]S. Zhang and Z. Li, Phys. Rev. Lett. **93**, 127204 (2004).
[15]A. Thiaville, Y. Nakatani, J. Miltat, and Y. Suzuki, Europhys. Lett. **69**, 990 (2005).
[16]L. Heyne, J. Rhensius, D. Ilgaz, A. Bisig, U. Rudiger, M. Klaui, L. Joly, F. Nolting, L. J. Heyderman, J. U. Thiele, and F. Kronast, Phys. Rev. Lett. **105**, 187203 (2010).
[17]K. Yamada, S. Kasai, Y. Nakatani, K. Kobayashi, and T. Ono, Appl. Phys. Lett. **93**,152502 (2008).
[18]K. Yamada, S. Kasai, Y. Nakatani, K. Kobayashi, and T. Ono, Appl. Phys. Lett. **96**, 192508 (2010).
[19]G. S. D. Beach, M. Tsoi, and J. L. Erskine, J. Magn. Magn. Mater. **320**, 1272 (2008).
[20]T. L. Gilbert, Phys. Rev. **100**, 1243 (1955).
[21]W. H. Press, B. P. Flannery, B. P. Teukolsky, S. A. Vetterling, and T. William, *Numerical Recipes in C: The Art of Scientific Computing* (Cambridge University Press, Cambridge, 1992).
[22]R. C. O'Handley, *Modern Magnetic Materials* (Wiley-Interscience, New York, 1999), Chap. 15.
[23]S. Kasai, Y. Nakatani, K. Kobayashi, H. Kohno, and T. Ono, Phys. Rev. Lett. **97**, 107204 (2006).
[24]R. Courant, K. Friedrichs, and H. Lewy, Phys. Math. Ann. **100**, 32 (1928).
[25]H. Gould and J. Tobochnik, *An Introduction to Computer Simulation Methods* (Addison-Wesley, Reading, MA, 1996), Chap. 10.
[26]R. A. Silva, T. S. Machado, G. Cernicchiaro, A. P. Guimaraes, and L. C. Sampaio, Phys. Rev. B **79**, 134434 (2009).
[27]P. Vavassori, M. Grimsditch, V. Metlushko, N. Zaluzec, and B. Ilic, Appl. Phys. Lett. **87**, 072507 (2005).
[28]H. Li, Y. Jiang, Y. Kawazoe, and R. Tao, Phys. Lett. A **298**, 410 (2002).
[29]M. Bolte, M. Steiner, C. Pels, M. Barthelmess, J. Kruse, U. Merkt, G. Meier, M. Holz, and D. Pfannkuche, Phys. Rev. B **72**, 224436 (2005).
[30]M. Holz, O. Kronenwerth, and D. Grundler, Phys. Rev. B **67**, 195312 (2003).
[31]J. Ohe, S. E. Barnes, H.-W. Lee, and S. Maekawai, Appl. Phys. Lett. **95**, 123110 (2009)
[32]L. K. Bogart and D. Atkinson, Appl. Phys. Lett. **94**, 042511 (2009).
[33]K. Y. Guslienko, K. S. Lee, and S. K. Kim, Phys. Rev. Lett. **100**, 027203 (2008).